Published by Institute of Physics Publishing for SISSA/ISAS
Received: *August 13, 2003*
Revised: *September 22, 2003*
Accepted: *September 24, 2003*

The resummation of inter-jet energy flow for gaps-between-jets processes at HERA

Robert B. Appleby and Mike H. Seymour

Theory Group, Department of Physics and Astronomy, Schuster Laboratory
University of Manchester, Manchester, UK, M13 9PL
E-mail: robert@theory.ph.man.ac.uk, seymour@theory.ph.man.ac.uk

Abstract: We calculate resummed perturbative predictions for gaps-between-jets processes and compare to HERA data. Our calculation of this non-global observable needs to include the effects of primary gluon emission (global logarithms) and secondary gluon emission (non-global logarithms) to be correct at the leading logarithm (LL) level. We include primary emission by calculating anomalous dimension matrices for the geometry of the specific event definitions and estimate the effect of non-global logarithms in the large N_c limit. The resulting predictions for energy flow observables are consistent with experimental data.

Keywords: QCD, Jets, Hadronic Colliders.

JHEP09(2003)056

Contents

1. Introduction

The subject of interjet energy flow [1] has attracted considerable interest ever since it was proposed [2, 3] as a way to study rapidity gap processes using the tools of perturbation theory. Rapidity gap processes are defined as processes containing two high p_t jets with the region of rapidity between the jets containing nothing more than soft radiation. This region is known generically as the gap. The presence of a range of scales offers a chance to study the interface between the soft, non-perturbative scales and the hard, perturbative scales of QCD.

In this paper we will calculate the perturbative contribution to gaps-between-jets cross sections in photoproduction at HERA, which have been measured by the ZEUS [4, 5] and H1 [6] collaborations. A feature of the recent analyses is the use of a clustering algorithm to define the hadronic final state and hence the gap. The restriction of transverse radiation in a region of phase space, defined as Ω and directed away from the observed jets and the beam directions, produces logarithms at each order of QCD perturbation theory of the interjet energy flow, Q_Ω, over some hard scale, Q. The precise definition of the restricted region, or gap, is totally free and in this work we are interested in the gap region defined by experimental rapidity gap analyses. The source of the large logarithms is twofold. The so-called primary (or global) logarithms arise from radiation emitted directly into Ω; these wide-angle gluons decouple from the dynamics of the colour-singlet jets and are described by an effective, eikonal theory [7]–[11]. The second source of leading logarithms arise from gluons emitted outside of the gap region, an area of phase space generically denoted as $\bar{\Omega}$, which subsequently radiate into Ω. These terms are known as non-global (secondary) logarithms, or NGLs [12]–[15].

The primary logarithms are resummed using the formalism of Collins, Soper and Sterman (CSS) [7, 16, 17, 18]. In this method the cross section is factorised into a soft part describing the emission of soft, wide angle gluons up to scale Q_Ω and a hard part, describing harder quanta. A unique feature of QCD is that the soft and the hard functions are expressed as matrices in the space of possible colour flow of the system. The scale invariance and factorisation properties of the cross section are then exploited to resum primary logarithms of Q_Ω/Q. This resummation is driven by the ultraviolet pole parts of eikonal Feynman graphs and we write the resummed cross section in terms of the eigenvalues of Ω-dependent soft anomalous dimension matrices. These matrices are known for gap definitions based on the cone definition of the final state [9, 10] and for a gap defined as a square patch in rapidity and azimuthal angle [11]; here we are interested in gaps defined in terms of the clustering algorithms employed in the recent analyses. Hence we are required to calculate the corresponding anomalous dimension matrices.

The NGLs [12, 13] are unable to be incorporated into the resummation of the primary logarithms, because the gluon emission patterns that produce the NGLs are sensitive to underlying colour flows not included in the formalism. The effect of NGLs, which is a suppressive effect, on energy flow processes has been studied using numerical methods in the large N_c limit and overall factors describing their effect have been extracted for a two jet system, both without [13] and with [14] clustering. This factor is not directly applicable to the 4 jet systems[1] relevant in the photoproduction of jets but, in the lack of a four jet formalism, we nevertheless use the two-jet factor in our predictions.

Our aim is to derive LL resummed predictions for the gap cross section, with primary logarithms correct to all orders and secondary logarithms correct in the large N_c limit. The gap cross section will follow the HERA analyses and demand two hard jets, defined using the kt clustering algorithm [19, 20, 21], and we will closely follow the H1 and ZEUS gap

[1]Note that for a two-to-two process the incoming and outgoing partons radiate, so we consider the process to be of "four jet" type, although only two jets are seen in the final state.

definition. The technical aspects of soft gluon resummation give a strong dependence on the gluon emission phase space, and hence a considerable part of our work will be concerned with the calculation of soft gluon effects for the specific detector geometry of the H1 and ZEUS experiments.

The organisation of this paper is as follows. Section 2 describes, in detail, the energy flow analyses of H1 and ZEUS. We describe the experimental cuts employed and the range of measured observables. We also discuss the theoretical implementation of the inclusive kt algorithm employed to define the hadronic final state and the impact on soft gluon resummation. Section 3 describes the theoretical definition of our cross section and we employ the standard QCD factorisation theorems to write it as the convolution of non-perturbative parton distributions and a short-distance hard scattering function. We then proceed to refactorise the hard scattering function and exploit this factorisation to resum the large interjet logarithms. Section 4 then derives the soft anomalous dimension matrices for the kt defined final state and in section 5 we present detailed predictions of rapidity gap processes and compare to the H1 data. Finally we draw our conclusion in section 6. We find that our description of the data is good, although the approximate treatment of NGLs results in a relatively large normalisation uncertainty.

2. The HERA energy flow analyses

In this section we will outline the experimental analyses of the photoproduction of gaps-between-jets processes and discuss the experimental cuts and rapidity gap observables. We will also describe the clustering algorithm used to define the final hadronic state in the more recent ZEUS [5] and H1 [6] analyses.

The data for these events were collected when HERA collided 27.6 GeV positrons[2] with 820 GeV protons, giving a centre of mass energy of $\sqrt{s} \simeq 300$ GeV. Following the jet-finding phase, which we will comment on later, the total transverse energy flow between the two highest E_T jets, denoted E_T^{GAP}, is calculated by summing the transverse energy of all particles that are not part of the dijets in the pseudorapidity region between the two highest jets. An event is then defined as a gap event if the energy is less than some energy cut $E_T^{\mathrm{CUT}} \equiv Q_\Omega$. A gap fraction is then calculated by dividing the cross section at fixed E_T^{CUT} by the inclusive cross section. The ZEUS collaboration performed a rapidity gap analysis several years ago [4] using the cone algorithm for the jet definition and presented the gap fraction at $Q_\Omega = 0.3$ GeV. We consider this value of Q_Ω as being too small for our perturbative analysis and will not make any predictions for this data set. The more recent H1 and ZEUS analyses used the kt definition of the final state and both collaborations presented the gap fraction at four different values of Q_Ω, as shown in table 1. We will make predictions and compare to data for the H1 data sets and, due to the fact that the ZEUS data is still preliminary, confine ourselves to making predictions for the ZEUS analysis. We have summarised the cuts used in table 1.

[2]The positron energy varied a negligible amount between the two sets of analyses.

	H1	ZEUS
E_T^{jet1}	$> 6.0\,\mathrm{GeV}$	$> 6.0\,\mathrm{GeV}$
E_T^{jet2}	$> 5.0\,\mathrm{GeV}$	$> 5.0\,\mathrm{GeV}$
η^{jet1}	< 2.65	< 2.4
η^{jet2}	< 2.65	< 2.4
$\Delta\eta$	$2.5 < \Delta\eta < 4$	$2 < \Delta\eta < 4$
η_{jj}	N/A	< 0.75
y	$0.3 < y < 0.6$	$0.2 < y < 0.85$
Q^2	$< 0.01\,\mathrm{GeV}^2$	$< 1\,\mathrm{GeV}^2$
jet def.	kt	kt
gap def.	$\Delta y = \Delta\eta$	$\Delta y = \Delta\eta$
R	1.0	1.0
Q_Ω	$0.5, 1.0, 1.5, 2.0\,\mathrm{GeV}$	$0.5, 1.0, 1.5, 2.0\,\mathrm{GeV}$

Table 1: The experimental cuts used for the HERA analyses.

2.1 The kt algorithm

Of special interest to those going about soft gluon calculations is the method used to define the hadronic final state, the reason being that this jet-finding process determines the phase space for soft gluon emission; the method used in the H1 and ZEUS data sets is the inclusive kt algorithm [19, 20, 21]. In this algorithm the final state is represented by a set of "protojets" i with momenta p_i^μ and works in an iterative way, grouping pairs of protojets together to form new ones. The aim is to group almost-parallel protojets together so that they are part of the same protojet. Once certain criteria are met, a protojet is considered a jet and is not considered further. Here we follow the so-called inclusive scheme used at H1 and ZEUS which depends on the parameter R, normally set to unity. If we assume that any radiation into the gap is much softer than any parent radiation, then this radiation with $E_T < E_T^{\mathrm{jet}}$ will be merged into the jet (with kinematical variables $(\eta_{\mathrm{jet}}, \phi_{\mathrm{jet}})$) if it satisfies

$$(\eta_r - \eta_{\mathrm{jet}})^2 + (\phi_r - \phi_{\mathrm{jet}})^2 < R^2\,, \tag{2.1}$$

where we denote the kinematical variables of the radiated gluon by (η_r, ϕ_r). Once merged, a gluon will be pulled out of the gap and can no longer produce a primary or secondary logarithm. The gap is defined as the interjet region minus the region of clustered radiation around the jets and may contain soft protojets. The gap transverse energy is then defined by the (scalar) sum of the protojets within the gap region, $\eta_1 < \eta < \eta_2$.

The kt gap definition can be contrasted to the older ZEUS analysis [4], which used the well known cone definition of the final state with $R = 1.0$. The gap transverse energy is then defined as the scalar sum of the hadrons within it, $\eta_1 + R < \eta < \eta_2 - R$.

JHEP09(2003)056

3. Factorisation, refactorisation and resummation of the cross section

In this section we will exploit the standard factorisation theorems of QCD to write down the dijet production cross section from the interaction of a proton and a positron. We will then refactorise the hard scattering function into the product of two matrices in the space of possible hard scattering colour flow, one matrix describing soft gluons radiated into the gap region and the other a hard scattering matrix. The renormalisation properties of the cross section are then used to resum primary interjet logarithms, and write the result in terms of the eigenvalues of the matrix of counterterms used to renormalise the soft function. In the following section we will calculate these matrices and their eigenvalues.

3.1 Photoproduction cross sections

The scattering of positrons and protons at HERA proceeds predominantly through the exchange of photons with very small virtuality and produces a large subset of events with jets of high transverse momentum, E_T. The presence of this large scale allows the application of the perturbative methods of QCD to predict the cross section for multiple jet production. This process is otherwise known as jet photoproduction.

The leading order (LO) QCD contribution can be divided into two types [9]. The first is the direct process in which the photon interacts directly with a parton from the proton and proceeds through either the Compton process, $\gamma q \to gq$, or the photon-gluon fusion process, $\gamma g \to q\bar{q}$. The second contribution is the resolved contribution, in which the virtual photon fluctuates into a hadronic state that acts as a source of partons, which then scatter off the partonic content of the proton. Therefore the reaction proceeds through standard QCD $2 \to 2$ parton scattering processes. Note that the precise determination of the partonic content of the photon is a very open question and there is a relatively large error associated with the photonic parton densities. The spectrum of virtual photons is approximated by the Weizäcker–Williams [22] formula,

$$F_{\gamma/e}(y) = \frac{\alpha}{2\pi}\frac{(1+(1-y)^2)}{y}\log\left(\frac{Q^2_{\max}(1-y)}{m_e^2 y^2}\right), \tag{3.1}$$

where m_e is the electron mass, y is the fraction of the positron's energy that is transfered to the photon, and $Q^2_{\max}$ is the maximum virtuality of the photon, which is determined by the experimental cuts employed in the analyses. Then, by using the equivalent photon approximation, the cross section for the process $e^+p \to e^+X$ is given by the convolution

$$\mathrm{d}\sigma(e^+p \to e^+X) = \int_{y_{\min}}^{y_{\max}} \mathrm{d}y\, F_{\gamma/e}(y)\, \mathrm{d}\sigma(\gamma p \to X)\,, \tag{3.2}$$

where we write $\mathrm{d}\sigma(\gamma p \to X)$ for the cross section of $\gamma p \to X$. The centre of mass energy squared for the photon-proton system is $W^2 = ys$, where s is the centre of mass energy squared for the positron-proton system. At HERA, $s \simeq 90{,}000\,\mathrm{GeV}^2$ and the values for $y_{\min}$ and $y_{\max}$ are determined by the experimental analyses. We can now write down the specific expression for the production of two high E_T jets from the photon-proton system, which is written as a sum of the direct and resolved contributions,

$$d\sigma_{e^+p}(s,\hat{t},\Delta\eta,\alpha_s(\mu_r),Q_\Omega) = \int_{y_{\min}}^{y_{\max}} \mathrm{d}y\, F_{\gamma/e}(y)\Big(\mathrm{d}\sigma^{\mathrm{dir}}_{\gamma p}\left(s_{\gamma p},\hat{t},\Delta\eta,\alpha_s(\mu_r),Q_\Omega\right) + \\ + \mathrm{d}\sigma^{\mathrm{res}}_{\gamma p}\left(s_{\gamma p},\hat{t},\Delta\eta,\alpha_s(\mu_r),Q_\Omega\right)\Big)\,, \quad (3.3)$$

where we denote the 4-momentum transfer squared in the hard scattering as $\hat{t}$. We define the rapidity separation and difference of the two hard jets by

$$\begin{aligned}\Delta\eta &= |\eta_1 - \eta_2|\,,\\ \eta_{JJ} &= \frac{1}{2}(\eta_1+\eta_2)\,.\end{aligned} \quad (3.4)$$

At this point we can appeal to the collinear factorisation theorems of QCD and, by working in the γp frame, write down factorised forms for the direct and resolved cross sections. The factorised direct cross section is

$$\frac{\mathrm{d}\sigma^{\mathrm{dir}}_{\gamma p}}{\mathrm{d}\hat{\eta}}\left(s_{\gamma p},\hat{t},\Delta\eta,\alpha_s(\mu_r),Q_\Omega\right) = \sum_{f_p,f_1,f_2}\int_{\mathrm{R_d}} \mathrm{d}x_p\,\phi_{f_p/p}(x_p,\mu_f)\times \\ \times\frac{\mathrm{d}\hat{\sigma}^{(\gamma f)}}{\mathrm{d}\hat{\eta}}(\hat{s},\hat{t},\Delta\eta,\alpha_s(\mu_r),Q_\Omega,\mu_f)\,, \quad (3.5)$$

and the factorised resolved cross section is

$$\frac{\mathrm{d}\sigma^{\mathrm{res}}_{\gamma p}}{\mathrm{d}\hat{\eta}}(s_{\gamma p},\hat{t},\Delta\eta,\alpha_s(\mu_r),Q_\Omega) = \sum_{f_\gamma,f_p,f_1,f_2}\int_{\mathrm{R_r}} \mathrm{d}x_\gamma\,\mathrm{d}x_p\,\phi_{f_\gamma/\gamma}(x_\gamma,\mu_f)\phi_{f_p/p}(x_p,\mu_f)\times \\ \times\frac{\mathrm{d}\hat{\sigma}^{(f)}}{\mathrm{d}\hat{\eta}}(\hat{s},\hat{t},\Delta\eta,\alpha_s(\mu_r),Q_\Omega,\mu_f)\,, \quad (3.6)$$

which are written in terms of the jet rapidity, $\hat{\eta}$, in the partonic centre-of-mass frame, and we write the factorisation scale and the renormalisation scale as μ_f and μ_r respectively. Note that $\hat{\eta} = \Delta\eta/2$, $\hat{s} = x_p W^2$ for the direct case and $\hat{s} = x_\gamma x_p W^2$ for the resolved case. In these equations we denote the integration regions of the direct and resolved convolutions, which are defined by the experimental cuts, by $\mathrm{R_d}$ and $\mathrm{R_r}$. The parton distribution for a parton of flavour f in the photon and the proton are denoted by $\phi_{f/\gamma}(x_\gamma,\mu_f)$ and $\phi_{f/p}(x_p,\mu_f)$ respectively and finally $\mathrm{d}\hat{\sigma}^{(\gamma f)}/\mathrm{d}\hat{\eta}$ and $\mathrm{d}\hat{\sigma}^{(f)}/\mathrm{d}\hat{\eta}$ are the hard scattering functions which, at lowest order, start from the Born cross sections. These are the functions that will contain the logarithmic enhancements of Q_Ω/Q, and hence depend on the definition of the gap Ω and the gap energy flow Q_Ω. We assume that Q_Ω is sufficiently soft that we can ignore the effects of emission on the parent jet, known as recoil, but large enough that $Q_\Omega^2 \gg \Lambda_{QCD}^2$. The index f denotes the process $f_\gamma + f_p \to f_1 + f_2$ and the index $f\gamma$ denotes the process $\gamma + f_p \to f_1 + f_2$. Since the aim of this paper is to calculate ratios of cross sections and compare with data, we will take the renormalisation scale to equal the factorisation scale and set $\mu_f = \mu_r = p_t$, where p_t is the transverse momentum of the produced jets.

JHEP09(2003)056

3.2 Refactorisation

Following [11, 7] we now refactorise the $2 \to 2$ hard scattering function into a hard matrix and a soft matrix,

$$\frac{d\hat{\sigma}^{(f)}}{d\hat{\eta}}\left(\hat{s},\hat{t},\Delta\eta,\alpha_s(\mu_r),Q_\Omega,\mu_f\right) = \sum_{L,I} H_{IL}^{(f)}\left(\hat{s},\hat{t},\Delta\eta,\alpha_s(\mu_r),\mu_f,\mu\right) S_{LI}^{(f)}(Q_\Omega,\alpha_s(\mu_r),\mu). \tag{3.7}$$

We introduce a factorisation scale μ, separate to the parton distribution factorisation scale μ_f, and all dynamics at scales less than μ are factored into S_{LI}. Therefore H_{IL} is Q_Ω independent, and all the Q_Ω dependence is included in S_{LI}. This latter function describes the soft gluon dynamics. The proof of this statement follows standard factorisation arguments [7]. The indices I and L label the basis of colour tensors which describe the possible colour exchange in the hard scattering, over which the hard and soft matrices are expressed. Soft, wide angle radiation decouples from the dynamics of the hard scattering and can be approximated by an effective cross section and in this effective theory the partons are treated as recoilless sources of gluonic radiation and replaced by eikonal lines, or path ordered exponentials of the gluon field [8]. The soft radiation pattern of this effective eikonal theory then mimics the radiation pattern of the partons participating in the hard event, or in other words the effective eikonal theory will contain the same logarithms of the soft scale as the full theory. The hard scattering function will begin at order α_s^2 for the resolved process and order $\alpha\alpha_s$ for the direct process, and the soft function will begin at zeroth order. The lowest order soft function, denoted S_{LI}^0, reduces to a set of colour traces. Note that the definition of the gap, and hence the soft function, depends on the jet separation $\Delta\eta$ but we have suppressed this argument of the soft function for clarity.

The construction of the soft function, and in particular its renormalisation properties, have been extensively studied elsewhere [8, 7]. A non-local operator is constructed from a product of Wilson lines, which ties four lines (representing the four jet process) together with a colour tensor. This operator, which contains ultraviolet divergences and hence requires renormalisation, is used to construct a so-called eikonal cross section, which serves as an effective theory for the soft emission. By summing over intermediate states the eikonal cross section is free of potential collinear singularities. It is the ultraviolet renormalisation of the eikonal operator that allows colour mixing and the resummation of soft interjet logarithms.

3.3 Factorisation leads to resummation of soft logarithms

The partonic cross section, which has been factorised into a hard and a soft function, should not depend on the choice of the factorisation scale μ. This leads to the soft function obeying

$$\left(\mu\frac{\partial}{\partial\mu}+\beta(g_s)\frac{\partial}{\partial g_s}\right)\underline{\underline{S}} = -\underline{\underline{\Gamma_s}}^{\dagger}(\hat{\eta},\Omega)\underline{\underline{S}} - \underline{\underline{S}}\,\underline{\underline{\Gamma_s}}(\hat{\eta},\Omega)\,. \tag{3.8}$$

It is important to point out that we have deliberately ignored the complications of terms in this equation arising from radiation into $\bar{\Omega}$ [11], and only include radiation emitted by the soft function directly into Ω. The implication of ignoring these non-global terms is discussed in section 3.4, where we also describe how to include their effect in a different way. Therefore we have never included the, technically correct, $\bar{\Omega}$ argument of the soft function. The matrices $\Gamma_s(\hat{\eta}, \Omega)$ are process-dependent soft anomalous dimension matrices that depend on the details of the gap definition and the hard scattering. This equation is solved by transforming to a basis in which these matrices are diagonal and hence we require a knowledge of the eigenvectors and eigenvalues of the soft anomalous dimension matrices. We obtain the entries for $\Gamma_s(\hat{\eta}, \Omega)$ from the coefficients of the ultraviolet poles in the matrix of counterterms which renormalise the soft function; we can write this quantity as a sum over terms from different eikonal lines each with the form of a colour factor multiplied by a scaleless integral:

$$(Z_S)_{LI} = \sum_{i,j} (Z_S^{(ij)})_{LI} = \sum_{i,j} \mathcal{C}_{LI}^{(ij)} \omega^{(ij)} \, . \tag{3.9}$$

The eikonal momentum integrals are process independent, and only depend on i and j, the eikonal lines that are connected by the virtual gluon. The colour factor is found from consideration of the colour flow for a given process and the basis over which the colour flow is to be decomposed. The result is a basis- and process-dependent set of colour mixing matrices, which we have listed in appendix C, together with our choice of bases in appendix A. The colour mixing matrices have been obtained in [11, 23, 24] for all relevant subprocesses, and involves using SU(3) colour identities like

$$t^a_{ij} t^a_{kl} = \frac{1}{2} \delta_{il} \delta_{kj} - \frac{1}{2N_c} \delta_{ij} \delta_{kl} \tag{3.10}$$

for quark processes and

$$d_{abc} = 2 \left[\mathrm{Tr} \left(t^a t^c t^b \right) + \mathrm{Tr} \left(t^a t^b t^c \right) \right] , \tag{3.11}$$

$$f_{abc} = -2i \left[\mathrm{Tr} \left(t^a t^b t^c \right) - \mathrm{Tr} \left(t^a t^c t^b \right) \right] , \tag{3.12}$$

for gluon processes, to decompose one-loop graphs over a colour basis. We use the fact that the colour flow for a real graph is the same as the corresponding virtual graph, valid for primary emission.

Therefore we need to calculate the ultraviolet divergent contribution to the momentum function $\omega^{(ij)}$ from all contributing eikonal graphs. Working in the Feynman gauge there are two possible sources of divergence. The first is one loop eikonal graphs with a virtual gluon connecting eikonal lines i and j. From the eikonal Feynman rules listed in the appendix, these graphs will give a real and an imaginary contribution to Γ_s. Note that as we are working in the Feynman gauge the self energy diagrams ($\omega^{(ii)}$) give no contribution. The second source of ultraviolet divergences are the real emission diagrams, when the emitted gluon is directed out of the gap. This can produce an ultraviolet divergence in the eikonal graph as we only measure energy flow into the gap and are fully inclusive out of the gap. Hence the virtual graphs will only depend on the relative direction of the two eikonal lines and the real graphs will give a gap (and hence a jet algorithm) dependence. This sum over real and virtual eikonal graphs ensures that the soft function remains free of collinear divergences. The imaginary (and geometry independent) part of all our anomalous

JHEP09(2003)056

dimension matrices can be extracted from [8, 10, 11, 23], and the calculation for a cone-algorithm defined final state has been done in [10]. For the latter case, we have re-expressed their results in accordance with our notation in appendix E.

By performing the energy integral of the virtual graphs, we can combine the result with the corresponding real graph at the integrand level and obtain a partial cancellation. We can then write the total momentum part as an integral over the vetoed gap region and arrive at

$$\begin{aligned}\omega^{(ij)} &= I_r^{(ij)} + I_v^{(ij)} \\ &= -g_s^2 \Delta_i \Delta_k \beta_i \cdot \beta_j \int \frac{d^{d-1}k}{2|\vec{k}|(2\pi)^{d-1}} \theta(\vec{k}) \frac{1}{(\delta_i \beta_i \cdot k)(\delta_j \beta_j \cdot k)} + \\ &\quad + \delta_i \delta_j \Delta_i \Delta_j \frac{\alpha_s}{2\pi} \frac{i\pi}{2\epsilon} (1 - \delta_i \delta_j) \,, \end{aligned} \tag{3.13}$$

where we integrate over the gap region allowed by the kt algorithm. The notation $\delta_i = +1(-1)$ means that the gluon momentum, denoted k, flows in the same(opposite) direction as the momentum of eikonal line i, and $\Delta_i = +1$ if the eikonal line is a quark, or it is a gluon and the soft gluon is above it in the Feynman diagram, or -1 if the eikonal line is an antiquark, or it is a gluon and the soft gluon is below it. β_i denotes the 4-velocity of eikonal line i, the function $\theta(\vec{k}) = 1$ when the vector $\vec{k}$ is directed into the gap and in this paper we will use the dimensional regularisation convention $d = 4 - 2\epsilon$. The finite remainder is a result of the energy veto into the gap spoiling the real/virtual cancellation. Once we have obtained the momentum integrals for the kt defined final state we can construct the anomalous dimension matrices using the colour mixing matrices in the appendix. Consideration of the eigenvalues and eigenvectors of these matrices, together with the process-dependent hard and soft matrices (the full set of hard and soft matrices is shown in appendix B) allows the resummed cross section to be written down,

$$\frac{d\hat{\sigma}^{(f)}}{d\hat{\eta}} = \sum_{L,I} \bar{H}_{IL}^{0,(f)} \bar{S}_{LI}^{0,(f)} \exp\left\{ \frac{1}{\beta_0} (\hat{\lambda}_L^*(\hat{\eta}, \Omega) + \hat{\lambda}_I(\hat{\eta}, \Omega)) \int_{p_t}^{Q_\Omega} \frac{d\mu}{\mu} \beta_0 \alpha_s(\mu) \right\} , \tag{3.14}$$

which follows from the diagonalisation of the soft RG equation (3.8). We denote matrices in the diagonal basis by barred matrices, the eigenvalues of the anomalous dimension matrices by $\lambda_i = \alpha_s \hat{\lambda}_i$ and we write the lowest-order piece of the QCD beta function as $\beta_0 = (11N_c - 2n_f)/(6\pi)$. We will observe that, in agreement with [10], $\mathrm{Re}(\lambda) > 0$ for all physical channels and hence the resummed cross sections are suppressed relative to the fully inclusive cross section.

3.4 Non-global effects

As we have discussed in the last section, we have deliberately ignored terms arising from secondary radiation into Ω, or non-global logarithms (NGLs) [12]–[15]. Such terms arise from radiation at some intermediate scale, M, being emitted outside of Ω, i.e. into $\bar{\Omega}$, and then subsequently radiating into Ω. In energy flow observables such effects give rise to leading logarithms. Inclusion of NGLs in the formalism of the last section would result

JHEP09(2003)056

in an explicit M dependence of the soft function and a sensitivity to more complicated, $2 \to n$, colour flows for all $n > 2$. For further details see [11]. NG effects have been studied for a two-jet system by Dasgupta and Salam [12, 13] and by the current authors with the complication of clustering [14], and in the context of energy flow/event shape correlations by Dokshitzer and Marchesini [25] and Berger, Kúcs and Sterman [26].

The effect of NGLs for four-jet kinematics has not been explicitly calculated to date. The best that has been managed is a two-jet calculation in the large-N_c limit. The NG contributions to the gap cross section factorize into an overall suppression factor S^{NG}, making it smaller than would be predicted by the resummation of primary logarithms alone. In the absence of a complete calculation, we include the NGLs approximately, by using our all-order results in the large-N_c limit for S^{NG} in a two-jet system [14]. Since four-jet configurations are dominated, in the large-N_c limit and for large $\Delta\eta$, by colour flows in which two colour dipoles stretch across the gap region, we approximate the four-jet NG suppression factor by the square of the two-jet one.

We have reperformed our previous calculation for the kinematic range relevant to HERA and find that the variation of S^{NG} with $\Delta\eta$ is very weak, so we neglect it. The variation with Q_Ω is very strong on the other hand. S^{NG} is a function of t,

$$t = \frac{1}{2\pi\beta_0} \log\left(\frac{\alpha_s(Q_\Omega)}{\alpha_s(Q)}\right), \tag{3.15}$$

where $\beta_0 = (11C_A - 2n_f)/(6\pi)$, and is well-approximated by a gaussian in t. Thus if Q_Ω is too close to Λ_{QCD}, t varies rapidly with it and S^{NG} varies very rapidly.

Q_Ω [GeV]	$S^{NG}(t)^2$
0.5	$0.10^{+0.30}_{-0.10}$
1.0	$0.47^{+0.16}_{-0.22}$
1.5	$0.65^{+0.10}_{-0.13}$
2.0	$0.74^{+0.07}_{-0.08}$

Table 2: The non-global emission suppression factors for the 4-jet system, obtained from an all-orders calculation for $Q = 6\,\text{GeV}$.

It is impossible to quantify the uncertainties in this approximation, without a more detailed understanding of the underlying physics. To get an idea however, we estimate the possible size of higher order corrections, by varying the hard scale at which α_s is evaluated. To leading logarithmic accuracy, this is equivalent to varying the value of $\alpha_s(Q)$ by an amount proportional to its value. We therefore evaluate t, and hence $S^{NG}(t)^2$, using our central value of $\alpha_s(M_z) = 0.116$, which implies $\alpha_s(Q = 6\,\text{GeV}) = 0.196$, and with raised and lowered values $\alpha_s^{\text{up}}(6\,\text{GeV}) = 0.234$ and $\alpha_s^{\text{down}}(6\,\text{GeV}) = 0.158$. For $Q_\Omega = 1.0\,\text{GeV}$, for example, these values result in $t = 0.097^{+0.056}_{-0.032}$ and hence $S^{NG}(t)^2 = 0.47^{+0.16}_{-0.22}$. We show the results for all relevant values of Q_Ω in table 2. Note that $Q_\Omega = 0.5\,\text{GeV}$ is so low that the range of uncertainty in t extends beyond Λ_{QCD} and hence the estimate of S^{NG} extends to zero. We have not shown any results for the 1995 cone-based ZEUS energy flow analysis [4] because the low value of $Q_\Omega = 0.3\,\text{GeV}$ means that the central value of the NG suppression is already zero, indicating a breakdown of our perturbative approach.

The uncertainty on the secondary emission probability estimated in this way should be added to that on the primary emission probability, described in section 5. However, we will find that the secondary uncertainty generally dominates the two. This is therefore clearly an area that needs more work if more precise quantitative predictions are to be made.

JHEP09(2003)056

4. Soft gluon dynamics for a kt defined final state

We now evaluate the momentum integral, $\omega^{(ij)}$, over the gap region Ω. The region of integration is determined by the experimental geometry, in which the final state is defined by the kt algorithm, and we shall work with the quantity

$$\Omega_{\mathrm{kt}}^{(ij)} = \int_{\mathrm{kt}} d\eta \int_{\mathrm{kt}} \frac{d\phi}{2\pi} \frac{\beta_i \cdot \beta_j}{(\beta_i \cdot \bar{k})(\beta_j \cdot \bar{k})}\,, \tag{4.1}$$

where we define $\bar{k} = k/k_t$. Therefore

$$\omega^{(ij)} = -\frac{\alpha_s}{2\pi} \Delta_i \Delta_j \delta_i \delta_j \frac{1}{2\epsilon} \Omega_{\mathrm{kt}}^{(ij)} + \mathrm{I.P.} \tag{4.2}$$

We denote the geometry independent imaginary part by $I.P.$, and we define the finite piece $\Gamma^{(ij)}$ by

$$\omega^{(ij)} = -\mathcal{S}_{ij} \frac{\Gamma^{(ij)}}{2\epsilon}\,. \tag{4.3}$$

We have extracted the sign function from $\Gamma^{(ij)}$,

$$\mathcal{S}_{ij} = \Delta_i \Delta_j \delta_i \delta_j\,, \tag{4.4}$$

so that

$$\Gamma^{(ij)} = \frac{\alpha_s}{2\pi} \Omega_{\mathrm{kt}}^{(ij)} + \mathrm{I.P.} \tag{4.5}$$

In this work we denote the rapidity separation of the jets by $\Delta\eta$ and the width of an azimuthally symmetric rapidity gap by Δy ($< \Delta\eta$). Therefore the available phase space for soft gluon emission for a kt defined final state is given by

$$\Omega_{\mathrm{kt}}^{(ij)} = \lim_{\Delta y \to \Delta\eta} \Big(\Omega_f^{(ij)}(\Delta y, \Delta\eta) - \Omega_1^{(ij)}(\Delta y, \Delta\eta, R) - \\ - \Omega_2^{(ij)}(\Delta y, \Delta\eta, R) \Big)\,, \tag{4.6}$$

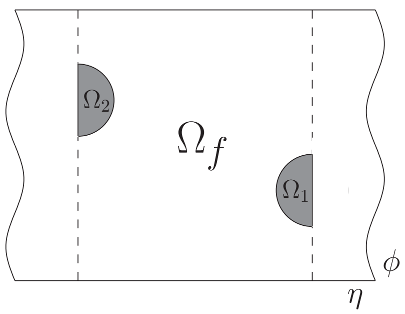

Figure 1: The phase space regions for a kt defined final state. The shading denotes the regions vetoed by the algorithm, which are subtracted from the Ω_f piece. Note that we have dropped the (ij) superscripts in this figure.

where the first term arises from an azimuthally symmetric gap of width Δy, and we subtract the region around each jet which is vetoed by the kt algorithm. The regions of this equation are shown in figure 1. In these regions any soft radiation is clustered into the jet, and cannot form part of Ω. In the first term we take Δy approaching $\Delta\eta$, and hence it contains a collinear divergence when the emitted gluon is collinear to one of the jets. The two subtracted pieces then remove the regions of phase space defined by

$$(\eta_k - \eta_i)^2 + (\phi_k - \phi_i)^2 < R^2\,, \tag{4.7}$$

where the index i labels final state jets and k labels the emitted gluon. The collinear divergences in the subtracted pieces exactly match the divergences in the first piece and hence the function $\Omega_{\rm kt}^{(ij)}(\Delta\eta)$ is collinear safe. Explicit definitions of the Ω functions are

$$\begin{aligned}\Omega_f^{(ij)} &= \int_{-\Delta y/2}^{+\Delta y/2} d\eta \int_0^{2\pi} \frac{d\phi}{2\pi} \frac{\beta_i \cdot \beta_j}{(\beta_i \cdot \bar{k})(\beta_j \cdot \bar{k})} \,, \\ \Omega_1^{(ij)} &= \int_{\Delta\eta/2-R}^{+\Delta y/2} d\eta \int_{-\phi_{\rm lim}}^{+\phi_{\rm lim}} d\phi \frac{\beta_i \cdot \beta_j}{(\beta_i \cdot \bar{k})(\beta_j \cdot \bar{k})} \,, \end{aligned} \tag{4.8}$$

where we write $\phi_{\rm lim} = \sqrt{R^2 - (\eta - \Delta\eta/2)^2}$ and obtain $\Omega_2^{(ij)}$ by the symmetry $\Omega_2^{(ij)} = \Omega_1^{(\bar{\imath}\bar{\jmath})}$, where the mapping $i \to \bar{\imath}$ is given by $\{a, b, 1, 2\} \to \{b, a, 2, 1\}$. If we define the following combinations of momentum integrals,

$$\begin{aligned}\alpha &= \mathcal{S}_{ab}\Gamma^{(ab)} + \mathcal{S}_{12}\Gamma^{(12)} \,, \\ \beta &= \mathcal{S}_{a1}\Gamma^{(a1)} + \mathcal{S}_{b2}\Gamma^{(b2)} \,, \\ \gamma &= \mathcal{S}_{b1}\Gamma^{(b1)} + \mathcal{S}_{a2}\Gamma^{(a2)} \,, \end{aligned} \tag{4.9}$$

where we have combined classes of diagram with the same colour structure, we obtain the following closed form for the positive gap contributions, in the limit $\Delta y \to \Delta\eta$,

$$\alpha = \frac{\alpha_s}{\pi}\left(2\Delta\eta + \log(1 - e^{-2\Delta\eta}) + \log\frac{1}{\Delta\eta - \Delta y} - 2i\pi\right) , \tag{4.10}$$

$$\beta = \frac{\alpha_s}{\pi}\left(\log(1 - e^{-2\Delta\eta}) + \log\frac{1}{\Delta\eta - \Delta y}\right) , \tag{4.11}$$

$$\gamma = \frac{\alpha_s}{\pi}\left(-2\Delta\eta - \log(1 - e^{-2\Delta\eta}) - \log\frac{1}{\Delta\eta - \Delta y}\right) . \tag{4.12}$$

The subtraction pieces are straightforward to express as power series in R and $e^{-\Delta\eta}$ and we shall illustrate the calculation of the momentum integrals with an example.

4.1 Calculation of $\Omega_{\rm kt}^{(a1)}$

We can write the matrix element in terms of the rapidity of the emitted gluon and obtain the following matrix element

$$\frac{\beta_i \cdot \beta_j}{(\beta_i \cdot \bar{k})(\beta_j \cdot \bar{k})} = \frac{e^{-\Delta\eta/2}}{e^{-\eta}(\cosh(\Delta\eta/2 - \eta) - \cos\phi)} \,. \tag{4.13}$$

The integrations for the function $\Omega_f^{(a1)}$ are straightforward, and we obtain

$$\Omega_f^{(a1)} = -\Delta y + \log\left(\frac{\sinh(\Delta\eta/2 + \Delta y/2)}{\sinh(\Delta\eta/2 - \Delta y/2)}\right) . \tag{4.14}$$

The expression for $\Omega_1^{(a1)}$ is

$$\Omega_1^{(a1)} = \int_{\Delta\eta/2-R}^{+\Delta y/2} d\eta \int_{-\phi_{\rm lim}}^{+\phi_{\rm lim}} \frac{d\phi}{2\pi} \frac{e^{-\Delta\eta/2}}{e^{-\eta}(\cosh(\Delta\eta/2 - \eta) - \cos\phi)} \,,$$

$$
\begin{aligned}
&= \int_{\Delta\eta/2-R}^{+\Delta y/2} d\eta \, f(\eta, \Delta\eta, R)\,, \\
&= \int_{\Delta\eta/2-\Delta y/2}^{R} d\eta' \, f(\eta', \Delta\eta, R)\,,
\end{aligned} \tag{4.15}
$$

where $\phi_{\lim}$ is defined in the previous section, we have performed the azimuthal integration in the second step and changed variable to $\eta' = \Delta\eta/2 - \eta$ in the third step. The function f can be easily obtained, but it is rather lengthy so we do not reproduce it here. We now note that this expression for $\Omega_1^{(ij)}$ only involves jet 1 and hence, by Lorentz invariance, cannot depend on the other jet and so may not be a function of the jet separation $\Delta\eta$. Therefore we write

$$
\Omega_1^{(a1)} = \int_{\Delta\eta/2-\Delta y/2}^{R} d\eta' \, f(\eta', R)\,. \tag{4.16}
$$

This function $f(\eta', R)$ has a divergence as $\eta' \to 0$, so we add and subtract this divergence to obtain

$$
\Omega_1^{(a1)} = \int_{\Delta\eta/2-\Delta y/2}^{R} d\eta' \left(f(\eta', R) - \frac{1}{\eta'} \right) + \int_{\Delta\eta/2-\Delta y/2}^{R} \frac{d\eta'}{\eta'}\,. \tag{4.17}
$$

We can rewrite the lower limit of the first, divergence free, integral as 0, and the collinear divergence is now contained in the second term. Therefore we have used Δy as a cut-off for the divergence, and we can write

$$
\Omega_1^{(a1)} = \bar{\Omega}_1^{ij} + \log 2R - \log(\Delta\eta - \Delta y)\,. \tag{4.18}
$$

We will always denote the divergence free angular integration, which always results from such a subtraction, as a barred quantity. We can now rescale the $\bar{\Omega}_1^{(a1)}$ integral, using $\bar{\eta} = \eta'/R$, to obtain

$$
\bar{\Omega}_1^{(a1)} = \int_0^1 d\bar{\eta} \left(R \cdot g(\bar{\eta}, R) - \frac{1}{\bar{\eta}} \right). \tag{4.19}
$$

This quantity, which is only a function of R, can now be expressed as a power series in R and the integrals done on a term-by-term basis. Doing this we obtain the rapidly converging series,

$$
\bar{\Omega}_1^{(a1)} = -\log(2) - \frac{2R}{\pi} + \frac{R^2}{8} - \frac{R^3}{18\pi} + \frac{R^4}{576} - \frac{R^5}{5400\pi} - \frac{R^7}{529200\pi} + \frac{R^8}{4147200} + \cdots\,. \tag{4.20}
$$

To calculate $\Omega_2^{(a1)}$ we use the parity symmetry and obtain the expression,

$$
\begin{aligned}
\Omega_2^{(a1)} &= \Omega_1^{(b2)} \\
&= \int_{\Delta\eta/2-R}^{+\Delta y/2} d\eta \int_{-\phi_{\lim}}^{+\phi_{\lim}} \frac{d\phi}{2\pi} \frac{e^{-\Delta\eta/2}}{e^{\eta}(\cosh(\Delta\eta/2+\eta) + \cos\phi)}\,.
\end{aligned} \tag{4.21}
$$

We now perform similar manipulations to the case of $\Omega_1^{(a1)}$. However, as $\Omega_2^{(a1)}$ is a function of both final state jets, the resulting expression must be a function of $\Delta\eta$ and we also note that $\Omega_2^{(a1)}$ is not divergent. We hence obtain the expression

$$
\bar{\Omega}_2^{(a1)} = \int_0^1 d\bar{\eta} \left(R \cdot f(\bar{\eta}, \Delta\eta, R) \right), \tag{4.22}
$$

which we can expand as a power series in the variables R and $z = \exp(-\Delta\eta)$, and perform the remaining integrations term-by-term.

The pole arising in the subtraction term $\Omega_1^{(a1)}$ now cancels against an equivalent pole in the function $\Omega_f^{(a1)}$, when we expand the latter in Δy around the point $\Delta\eta$,

$$\lim_{\Delta y \to \Delta\eta} \Omega_f^{(a1)} \sim -\Delta\eta - \log(\Delta\eta - \Delta y) + \log(2\sinh\Delta\eta)\,. \tag{4.23}$$

Therefore we find the final, divergence free, form of $\Omega_{\mathrm{kt}}^{(a1)}$ as

$$\Omega_{\mathrm{kt}}^{(a1)} = -\Delta\eta + \log(2\sinh\Delta\eta) - \log(2R) - \bar{\Omega}_1^{(a1)} - \bar{\Omega}_2^{(a1)}\,. \tag{4.24}$$

We have presented the full set of series expansions in appendix D and these, together with equations (4.10)–(4.12), are sufficient to compute the set of kt defined momentum integrals and hence the corresponding anomalous dimension matrix. It is worth noting that, although the off-diagonal terms for the kt anomalous dimension matrices are no longer pure imaginary as in the cone case, their real parts still vanish for large $\Delta\eta$. Indeed for $\Delta\eta = 2$, the real part is more than two orders of magnitude smaller than the imaginary part. We have listed the closed-form momentum integrals for the cone defined final state using our notation in appendix E.

5. Results

We now have the tools we need to calculate resummed cross sections at HERA, which correctly include primary emission to all orders and secondary emission approximately in the large N_c limit. The colour bases used for the contributing partonic cross sections are presented in the appendix, along with the decomposed hard and soft matrices. We also present the complete colour mixing matrices and the correct sign structure for the three classes of diagram. Therefore we can use the eigenvectors and eigenvalues of the soft anomalous dimension matrices, together with the hard and soft matrices, to calculate the primary resummed cross section using equation (3.14), for either a kt or a cone defined final state. The differential cross section, in $\Delta\eta$, can then be computed using the cuts given in section 2, both for the totally inclusive cross section (no gap) and for the gap cross section at fixed Q_Ω. The gap fraction is then found by dividing the latter quantity by the former. All our results are computed using GRV photon parton densities [27] and the MRST proton parton densities [28]. We have included an estimate of the theoretical uncertainty in the primary resummation by varying the hard scale in the evaluation of α_s, while keeping the ratio of the hard and soft scales fixed.

5.1 Totally inclusive *ep* cross section and the gap cross section

The left hand side of figure 2 shows the totally inclusive dijet cross section for the H1 analysis and the gap cross section for $Q_\Omega = 1.0\,\mathrm{GeV}$. We have not shown further values of Q_Ω as all the plots show qualitatively the same behaviour. We have cross-checked our total inclusive cross section against the Monte Carlo event generator HERWIG [29, 30] and we obtained complete agreement for the H1 and both the ZEUS sets of cuts. In figure 2 the solid curve is the total inclusive cross section, the dashed line is the cross section with the

JHEP09(2003)056

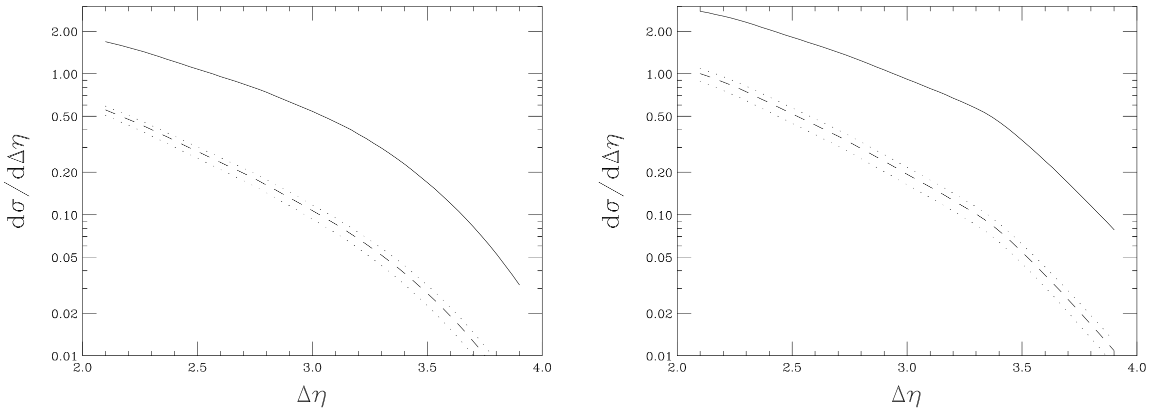

Figure 2: The cross sections for the H1 data (left) and the ZEUS data (right), which was defined using the kt algorithm with $R = 1.0$. On both plots the solid line is the total inclusive cross section, the dashed line is the gap cross section for $Q_\Omega = 1\,\mathrm{GeV}$ with only primary emission included, and the dotted lines indicate the range of theoretical uncertainty in the prediction.

primary interjet logarithms resummed and the dotted lines show the theoretical uncertainty of the primary resummation, estimated by varying α_s as described above. The inclusion of the primary gap logarithms gives a substantial suppression of the cross section; our analysis confirms simple "area of phase space" arguments which say that the kt defined final state will have greater soft gluon suppression than a cone defined final state due to the increased gap area in the (η, ϕ) plane. This plot for the ZEUS analysis is shown in the right hand side of figure 2.

5.2 Gap fractions

The gap fraction is defined as the gap cross section, at fixed Q_Ω, divided by the total inclusive cross section. Figure 3 shows the gap fraction for the H1 cuts at the four experimentally measured values of Q_Ω and figure 4 shows the gap fractions for the ZEUS analysis. The solid line is the gap fraction curve obtained by including the primary emission and the NG suppression factors of table 2 in the prediction for the gap cross section. The dotted lines show the theoretical uncertainty of both the primary and secondary emission probabilities, and the dashed line shows the gap fraction obtained by including only the primary emission contribution. We find that our gap fraction is consistent with the H1 values for the measured Q_Ω. The large uncertainty in the gap fraction predictions comes from an approximate treatment of the NG suppression and from using perturbation theory at $\sim 1\,\mathrm{GeV}$. Nonetheless, this uncertainty is principally in the normalisation of the curves and we expect our resummation to accurately describe the shape of the gap fraction curves.

6. Conclusions

In this paper we have computed resummed predictions for rapidity gap processes at HERA. We include primary logarithms using the soft gluon techniques of CSS, and include the effects of NGLs using an overall suppression factor computed from an extension of our earlier

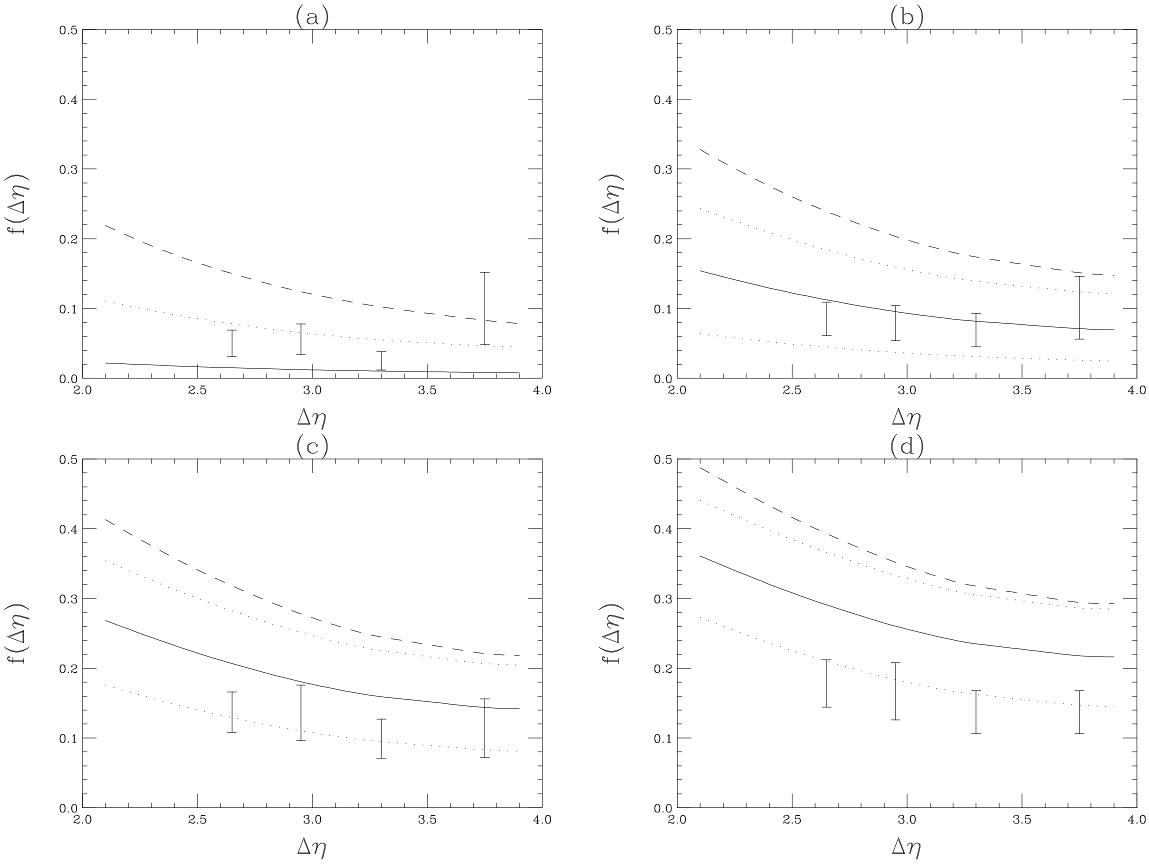

Figure 3: The gap fractions for the H1 analysis with a kt defined final state ($R = 1.0$), at varying Q_Ω. $Q_\Omega = 0.5$, 1.0, 1.5, 2.0 GeV for plots (a), (b), (c) and (d) respectively. The H1 data is also shown. The solid line includes the effects of primary emission and the secondary emission suppression factor. The overall theoretical uncertainty, including the primary uncertainty and the secondary uncertainty, is shown by the dotted lines. The dashed line indicates the gap fraction obtained by including only primary emission.

work. The kt definition of a hadronic final state determines the phase space available for soft primary emission and we have computed a set of anomalous dimension matrices specific to the geometry of the H1 and ZEUS analyses. Of course this method can be used for any definition of the gap, provided Ω is directed away from all hard jets. We then compared our predictions with gaps-between-jets data from the H1 collaboration and found a consistent agreement. The theoretical uncertainty of our predictions is relatively large, and generally dominated by the secondary emission uncertainty. However our resummed predictions correctly predict the shape of the H1 data, and the normalisation agrees within errors. There is a suggestion that the Q_Ω dependence is not quite right, with our central $Q_\Omega = 0.5$ GeV prediction below data and our central $Q_\Omega = 2.0$ GeV prediction above data, although all are within our uncertainty. It is possible that a more complete treatment of the perturbative/non-perturbative interface would improve this. We expect that calculation of primary emission will be correct if Q_Ω is not too large, so that we can neglect jet recoil. However our calculation is of sufficient accuracy in the region of phase space probed at HERA.

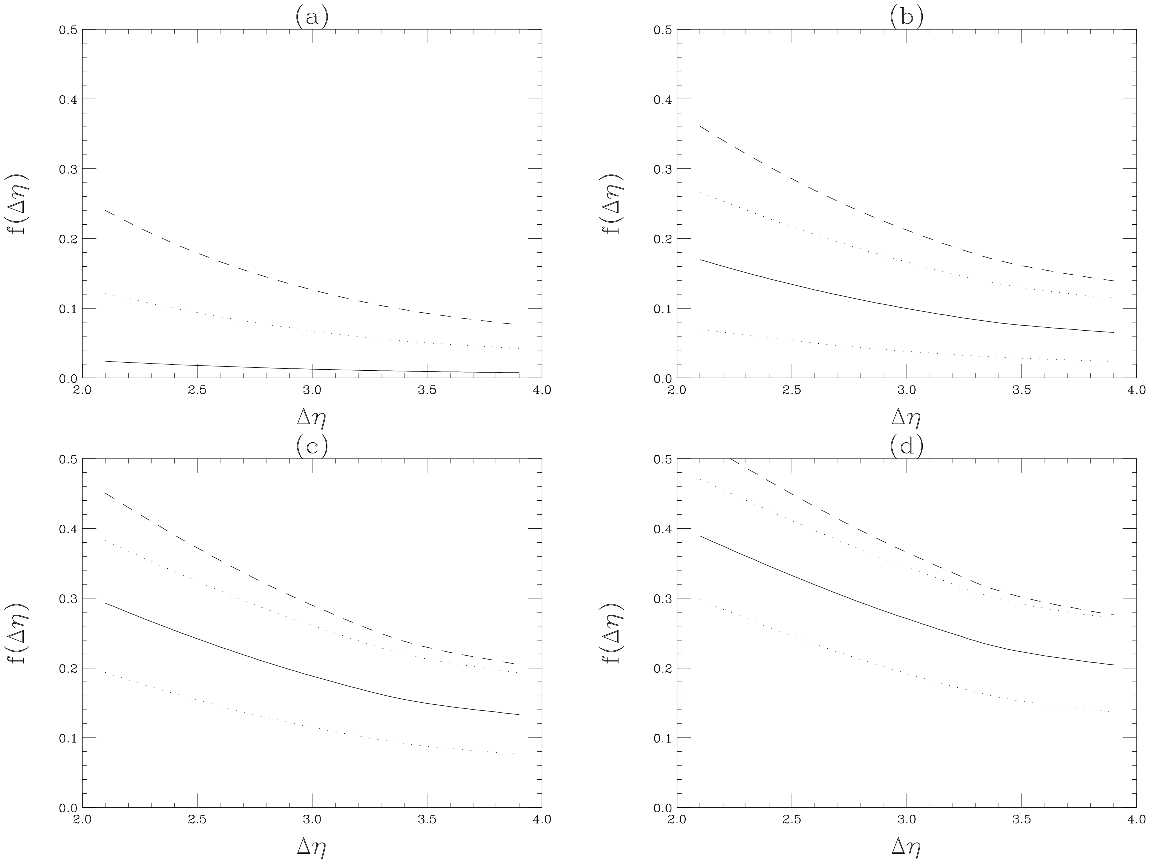

Figure 4: The gap fractions for the ZEUS analysis with a kt defined final state ($R = 1.0$), at varying Q_Ω. $Q_\Omega = 0.5$, 1.0, 1.5, 2.0 GeV for plots (a), (b), (c) and (d) respectively. The solid line includes the effects of primary emission and the secondary emission suppression factor. The overall theoretical uncertainty, including the primary uncertainty and the secondary uncertainty, is shown by the dotted lines. The dashed line indicates the gap fraction obtained by including only primary emission.

Our treatment of the NGLs is very approximate. For a fuller treatment, it is necessary to extend the extraction of the suppression factor to beyond the large N_c limit and overcome the inherent disadvantages of the numerical methods used. For the current application, consideration of the four jet system is also necessary. We reserve the latter extension, in the large N_c limit, for future work. Our calculation has not included power corrections [31]. The inclusion of such non-perturbative effects is required for a full and correct comparison to the experimental data. Again, we reserve this for future work.

Our calculation involves a numerical integration over all kinematic variables, so it would be straightforward to calculate the dependence of the gap fraction on, for example, the fraction of the photon's momentum participating in the hard process, x_γ. This code is available from the authors.

In conclusion, we have shown that the calculation of primary and secondary emission patterns can give a good description of rapidity gap data at HERA. A fuller treatment would refine our approximation of NGLs and include power corrections.

Acknowledgments

We are grateful to George Sterman and Carola Berger for useful communications and RBA would like to acknowledge the Particle Physics and Astronomy Research Council for financial support.

A. Colour bases

In this section we present the colour bases used in this work. All the bases in this section have appeared elsewhere [10, 11, 23, 24], but we show them here for completeness.

The process $q\bar{q} \to q\bar{q}$.

$$\begin{aligned} c_1 &= \delta_{a1}\delta_{b2}\,, \\ c_2 &= -\frac{1}{2N_c}\delta_{a1}\delta_{b2} + \frac{1}{2}\delta_{ab}\delta_{12}\,. \end{aligned} \tag{A.1}$$

The process $qq \to qq$.

$$\begin{aligned} c_1 &= \delta_{a1}\delta_{b2}\,, \\ c_2 &= -\frac{1}{2N_c}\delta_{a1}\delta_{b2} + \frac{1}{2}\delta_{a2}\delta_{b1}\,. \end{aligned} \tag{A.2}$$

The process $qg \to qg$.

$$\begin{aligned} c_1 &= \delta_{a1}\delta_{b2}\,, \\ c_2 &= d_{b2c}(T_F^c)_{1a}\,, \\ c_3 &= if_{b2c}(T_F^c)_{1a}\,. \end{aligned} \tag{A.3}$$

The processes $q\bar{q} \to gg$ and $gg \to q\bar{q}$. The process $gg \to q\bar{q}$ has the basis,

$$\begin{aligned} c_1 &= \delta_{ab}\delta_{12}\,, \\ c_2 &= d_{abc}(T_F^c)_{12}\,, \\ c_3 &= if_{abc}(T_F^c)_{12}\,. \end{aligned} \tag{A.4}$$

To find the basis for $q\bar{q} \to gg$, we interchange $a \leftrightarrow 2$ and $b \leftrightarrow 1$.

The process $gg \to gg$. The complete basis is

$$\left\{c_1, c_2, c_3, P_1, P_{8_S}, P_{8_A}, P_{10\oplus\overline{10}}, P_{27}\right\}, \tag{A.5}$$

where

$$\begin{aligned} c_1 &= \frac{i}{4}\left[f_{abc}d_{12c} - d_{abc}f_{12c}\right], \\ c_2 &= \frac{i}{4}\left[f_{abc}d_{12c} + d_{abc}f_{12c}\right], \\ c_3 &= \frac{i}{4}\left[f_{a1c}d_{b2c} + d_{a1c}f_{b2c}\right], \end{aligned}$$

$$
\begin{aligned}
P_1 &= \frac{1}{8}\delta_{a1}\delta_{b2}\,, \\
P_{8_S} &= \frac{3}{5}d_{a1c}d_{b2c}\,, \\
P_{8_A} &= \frac{1}{3}f_{a1c}f_{b2c}\,, \\
P_{10\bigoplus\overline{10}} &= \frac{1}{2}\left(\delta_{ab}\delta_{12}-\delta_{a2}\delta_{b1}\right)-\frac{1}{3}f_{a1c}f_{b2c}\,, \\
P_{27} &= \frac{1}{2}\left(\delta_{ab}\delta_{12}+\delta_{a2}\delta_{b1}\right)-\frac{1}{8}\delta_{a1}\delta_{b2}-\frac{3}{5}d_{a1c}d_{b2c}\,.
\end{aligned}
\tag{A.6}
$$

The direct processes. Since there is only one colour structure, these are basis independent.

B. The hard and soft matrices

We now show the complete set of hard and soft matrices used in this work. These matrices have appeared in a variety of forms in [10, 11, 23, 24]. In all these equations we have set $N_c = 3$ and have written the coupling scale as μ. Note that all our hard matrices differ from the normalisation used in [10, 23] by a factor of $\pi/(2\hat{s})\,4\hat{t}\hat{u}/\hat{s}^2$, while they agree with that used in [11].

The process $q\bar{q} \to q\bar{q}$. The hard matrix has, in the basis (A.1), the form

$$
H^{(1)} = \frac{1}{9}\frac{\alpha_s^2(\mu)\pi}{\hat{s}}\frac{4\hat{t}\hat{u}}{\hat{s}^2}\begin{pmatrix} \frac{16}{81}\chi_1 & \frac{4}{27}\chi_2 \\ \frac{4}{27}\chi_2 & \chi_3 \end{pmatrix}, \tag{B.1}
$$

where we define

$$
\begin{aligned}
\chi_1 &= \frac{\hat{t}^2+\hat{u}^2}{\hat{s}^2}\,, \\
\chi_2 &= 3\frac{\hat{u}^2}{\hat{s}\hat{t}}-\frac{\hat{t}^2+\hat{u}^2}{\hat{s}^2}\,, \\
\chi_3 &= \frac{\hat{s}^2+\hat{u}^2}{\hat{t}^2}+\frac{1}{9}\frac{\hat{t}^2+\hat{u}^2}{\hat{s}^2}-\frac{2}{3}\frac{\hat{u}^2}{\hat{s}\hat{t}}\,.
\end{aligned}
\tag{B.2}
$$

The unequal flavour process $q\bar{q}' \to q\bar{q}'$ is found by dropping the s-channel terms from these equations, and the unequal flavour process $q\bar{q} \to q'\bar{q}'$ is found by dropping the t-channel terms. The hard matrix for $q\bar{q} \to \bar{q}q$ is found using the transformation $\hat{t} \leftrightarrow \hat{u}$. The corresponding soft matrix for all these processes is

$$
S^{(0)} = \begin{pmatrix} N_c^2 & 0 \\ 0 & \frac{1}{4}(N_c^2-1) \end{pmatrix}. \tag{B.3}
$$

The process $qq \to qq$. The hard matrix has, in the basis (A.2), the form

$$
H^{(1)} = \frac{1}{9}\frac{\alpha_s^2(\mu)\pi}{\hat{s}}\frac{4\hat{t}\hat{u}}{\hat{s}^2}\begin{pmatrix} \frac{16}{81}\chi_1 & \frac{4}{27}\chi_2 \\ \frac{4}{27}\chi_2 & \chi_3 \end{pmatrix}, \tag{B.4}
$$

where we define

$$\chi_1 = \frac{\hat{t}^2+\hat{s}^2}{\hat{u}^2}\,,$$
$$\chi_2 = 3\frac{\hat{s}^2}{\hat{u}\hat{t}} - \frac{\hat{t}^2+\hat{s}^2}{\hat{u}^2}\,,$$
$$\chi_3 = \frac{\hat{u}^2+\hat{s}^2}{\hat{t}^2} + \frac{1}{9}\frac{\hat{t}^2+\hat{s}^2}{\hat{u}^2} - \frac{2}{3}\frac{\hat{s}^2}{\hat{u}\hat{t}}\,. \tag{B.5}$$

For the process $qq' \to qq'$ only keep the t-channel terms. The corresponding soft matrix is

$$S^{(0)} = \begin{pmatrix} N_c^2 & 0 \\ 0 & \frac{1}{4}(N_c^2-1) \end{pmatrix}. \tag{B.6}$$

The process $qg \to qg$. The hard matrix has, in the basis (A.3), the form

$$H^{(1)} = \frac{1}{24}\frac{\alpha_s^2(\mu)\pi}{2\hat{s}}\frac{4\hat{t}\hat{u}}{\hat{s}^2}\begin{pmatrix} \frac{1}{18}\chi_1 & \frac{1}{6}\chi_1 & \frac{1}{3}\chi_2 \\ \frac{1}{6}\chi_1 & \frac{1}{2}\chi_1 & \chi_2 \\ \frac{1}{3}\chi_2 & \chi_2 & \chi_3 \end{pmatrix}, \tag{B.7}$$

where we define

$$\chi_1 = 2 - \frac{\hat{t}^2}{\hat{s}\hat{u}}\,,$$
$$\chi_2 = 1 - \frac{1}{2}\frac{\hat{t}^2}{\hat{s}\hat{u}} - \frac{\hat{u}^2}{\hat{s}\hat{t}} - \frac{\hat{s}}{\hat{t}}\,,$$
$$\chi_3 = 3 - 4\frac{\hat{s}\hat{u}}{\hat{t}^2} - \frac{1}{2}\frac{\hat{t}^2}{\hat{s}\hat{u}}\,. \tag{B.8}$$

The hard matrix for the process $qg \to gq$ is found by the transformation $\hat{t} \leftrightarrow \hat{u}$. The corresponding soft matrix is

$$S^{(0)} = \begin{pmatrix} N_c(N_c^2-1) & 0 & 0 \\ 0 & \frac{1}{2N_c}(N_c^2-4)(N_c^2-1) & 0 \\ 0 & 0 & \frac{1}{2}N_c(N_c^2-1) \end{pmatrix}. \tag{B.9}$$

The processes $q\bar{q} \to gg$ and $gg \to q\bar{q}$. In the basis (A.4) the hard matrix for these processes has the form

$$H^{(1)} = \frac{1}{\Delta}\frac{\alpha_s^2(\mu)\pi}{2\hat{s}}\frac{4\hat{t}\hat{u}}{\hat{s}^2}\begin{pmatrix} \frac{1}{18}\chi_1 & \frac{1}{6}\chi_1 & \frac{1}{6}\chi_2 \\ \frac{1}{6}\chi_1 & \frac{1}{2}\chi_1 & \frac{1}{2}\chi_2 \\ \frac{1}{6}\chi_2 & \frac{1}{2}\chi_2 & \frac{1}{2}\chi_3 \end{pmatrix}, \tag{B.10}$$

where we define

$$\chi_1 = \frac{\hat{t}^2+\hat{u}^2}{\hat{t}\hat{u}}\,,$$
$$\chi_2 = \left(1+\frac{2\hat{t}}{\hat{s}}\right)\chi_1\,,$$
$$\chi_3 = \left(1-\frac{4\hat{t}\hat{u}}{\hat{s}^2}\right)\chi_1\,. \tag{B.11}$$

The constant $\Delta = 9$ for the process $q\bar{q} \to gg$ and $\Delta = 64$ for the process $gg \to q\bar{q}$. The matrix for the process $gg \to \bar{q}q$ is found from the transformation $\hat{t} \leftrightarrow \hat{u}$. The soft matrix is

$$S^{(0)} = \frac{N_c^2 - 1}{2N_c} \begin{pmatrix} 2N_c^2 & 0 & 0 \\ 0 & N_c^2 - 4 & 0 \\ 0 & 0 & N_c^2 \end{pmatrix}. \tag{B.12}$$

The process $gg \to gg$. The hard matrix, in the basis (A.5) has the block-diagonal form

$$H^{(1)} = \begin{pmatrix} 0_{3\times3} & 0_{3\times5} \\ 0_{5\times3} & H^{(1)}_{5\times5} \end{pmatrix}, \tag{B.13}$$

where the matrix $H^{(1)}_{5\times5}$ has the form

$$H^{(1)}_{5\times5} = \frac{1}{16}\frac{\alpha_s^2(\mu)\pi}{2\hat{s}}\frac{4\hat{t}\hat{u}}{\hat{s}^2} \begin{pmatrix} 9\chi_1 & \frac{9}{2}\chi_1 & \frac{9}{2}\chi_2 & 0 & -3\chi_1 \\ \frac{9}{2}\chi_1 & \frac{9}{4}\chi_1 & \frac{9}{4}\chi_2 & 0 & -\frac{3}{2}\chi_1 \\ \frac{9}{2}\chi_2 & \frac{9}{4}\chi_2 & \chi_3 & 0 & -\frac{3}{2}\chi_2 \\ 0 & 0 & 0 & 0 & 0 \\ -3\chi_1 & -\frac{3}{2}\chi_1 & -\frac{3}{2}\chi_2 & 0 & \chi_1 \end{pmatrix}, \tag{B.14}$$

and we write

$$\begin{aligned} \chi_1 &= 1 - \frac{\hat{t}\hat{u}}{\hat{s}^2} - \frac{\hat{s}\hat{t}}{\hat{u}^2} + \frac{\hat{t}^2}{\hat{s}\hat{u}}, \\ \chi_2 &= \frac{\hat{s}\hat{t}}{\hat{u}^2} - \frac{\hat{t}\hat{u}}{\hat{s}^2} + \frac{\hat{u}^2}{\hat{s}\hat{t}} - \frac{\hat{s}^2}{\hat{t}\hat{u}}, \\ \chi_3 &= \frac{27}{4} - 9\left(\frac{\hat{s}\hat{u}}{\hat{t}^2} + \frac{1}{4}\frac{\hat{t}\hat{u}}{\hat{s}^2} + \frac{1}{4}\frac{\hat{s}\hat{t}}{\hat{u}^2}\right) + \frac{9}{2}\left(\frac{\hat{u}^2}{\hat{s}\hat{t}} + \frac{\hat{s}^2}{\hat{t}\hat{u}} - \frac{1}{2}\frac{\hat{t}^2}{\hat{s}\hat{u}}\right). \end{aligned} \tag{B.15}$$

For this process the soft matrix is

$$S^{(0)} = \begin{pmatrix} 5 & 0 & 0 & 0 & 0 & 0 & 0 & 0 \\ 0 & 5 & 0 & 0 & 0 & 0 & 0 & 0 \\ 0 & 0 & 5 & 0 & 0 & 0 & 0 & 0 \\ 0 & 0 & 0 & 1 & 0 & 0 & 0 & 0 \\ 0 & 0 & 0 & 0 & 8 & 0 & 0 & 0 \\ 0 & 0 & 0 & 0 & 0 & 8 & 0 & 0 \\ 0 & 0 & 0 & 0 & 0 & 0 & 20 & 0 \\ 0 & 0 & 0 & 0 & 0 & 0 & 0 & 27 \end{pmatrix}. \tag{B.16}$$

The direct processes. For both these processes the zeroth order soft factor is unity and the hard functions are

$$\begin{aligned} H^{(1)}(\gamma g \to q\bar{q}) &= \left(\sum_q e_q^2\right) \frac{\alpha_s \alpha_{\rm em}\pi}{2\hat{s}}\frac{4\hat{t}\hat{u}}{\hat{s}^2}\left(\frac{\hat{u}}{\hat{t}} + \frac{\hat{t}}{\hat{u}}\right), \\ H^{(1)}(\gamma q(\bar{q}) \to gq(\bar{q})) &= \frac{8}{3}e_q^2\frac{\alpha_s \alpha_{\rm em}\pi}{2\hat{s}}\frac{4\hat{t}\hat{u}}{\hat{s}^2}\left(\frac{-\hat{u}}{\hat{s}} + \frac{\hat{s}}{-\hat{u}}\right), \end{aligned} \tag{B.17}$$

where e_q is the electric charge of quark flavour q, in units of the electron charge. Note that if the sum for $\gamma g \to q\bar{q}$ is taken to be over four flavours, then this gives a factor of 10/9.

C. Colour decomposition matrices

We now give the full set of colour decomposition matrices, and the sign function $\mathcal{S}$, defined by equation (4.4), for α, β and γ, defined by

$$\begin{aligned}\alpha &= \mathcal{S}_{ab}\Gamma^{(ab)} + \mathcal{S}_{12}\Gamma^{(12)}\,,\\ \beta &= \mathcal{S}_{a1}\Gamma^{(a1)} + \mathcal{S}_{b2}\Gamma^{(b2)}\,,\\ \gamma &= \mathcal{S}_{b1}\Gamma^{(b1)} + \mathcal{S}_{a2}\Gamma^{(a2)}\,.\end{aligned} \tag{C.1}$$

The process $q\bar{q} \to q\bar{q}$.

$$\mathcal{C}^{q\bar{q}\to q\bar{q}} = \begin{pmatrix} C_F\beta & \frac{C_F}{2N_c}(\alpha+\gamma) \\ \alpha+\gamma & C_F\alpha - \frac{1}{2N_c}(\alpha+\beta+2\gamma) \end{pmatrix}. \tag{C.2}$$

The signs are

$$\mathcal{S}_\alpha = +1\,, \tag{C.3}$$
$$\mathcal{S}_\beta = +1\,, \tag{C.4}$$
$$\mathcal{S}_\gamma = -1\,. \tag{C.5}$$

The process $qq \to qq$.

$$\mathcal{C}^{qq\to qq} = \begin{pmatrix} C_F\beta & \frac{C_F}{2N_c}(\alpha+\gamma) \\ \alpha+\gamma & C_F\gamma - \frac{1}{2N_c}(2\alpha+\beta+\gamma) \end{pmatrix}. \tag{C.6}$$

The signs are

$$\mathcal{S}_\alpha = -1, \tag{C.7}$$
$$\mathcal{S}_\beta = +1, \tag{C.8}$$
$$\mathcal{S}_\gamma = +1. \tag{C.9}$$

The process $qg \to qg$.

$$\mathcal{C}^{qg\to qg} = \begin{pmatrix} C_F\Gamma^{(a1)} + C_A\Gamma^{(b2)} & 0 & -\frac{1}{2}(\alpha+\gamma) \\ 0 & \chi & -\frac{N_c}{4}(\alpha+\gamma) \\ -(\alpha+\gamma) & -\frac{N_c^2-4}{4N_c}(\alpha+\gamma) & \chi \end{pmatrix}. \tag{C.10}$$

The signs are

$$\mathcal{S}_\alpha = +1\,, \tag{C.11}$$
$$\mathcal{S}_\beta = +1\,, \tag{C.12}$$
$$\mathcal{S}_\gamma = -1\,, \tag{C.13}$$

and we define

$$\chi = \frac{N_c}{4}(\alpha-\gamma) - \frac{1}{2N_c}\Gamma^{(a1)} + \frac{N_c}{2}\Gamma^{(b2)}\,. \tag{C.14}$$

The processes $q\bar{q} \to gg$ and $gg \to q\bar{q}$. For $q\bar{q} \to gg$ we have

$$\mathcal{C}^{q\bar{q}\to gg} = \begin{pmatrix} C_F\Gamma^{(ab)} + C_A\Gamma^{(12)} & 0 & \frac{1}{2}(\beta+\gamma) \\ 0 & \chi' & \frac{N_c}{4}(\beta+\gamma) \\ (\beta+\gamma) & \frac{N_c^2-4}{4N_c}(\beta+\gamma) & \chi' \end{pmatrix}. \tag{C.15}$$

The signs are

$$\mathcal{S}_\alpha = +1\,, \tag{C.16}$$
$$\mathcal{S}_\beta = +1\,, \tag{C.17}$$
$$\mathcal{S}_\gamma = -1\,, \tag{C.18}$$

and we define

$$\chi' = \frac{N_c}{4}(\beta-\gamma) - \frac{1}{2N_c}\Gamma^{(ab)} + \frac{N_c}{2}\Gamma^{(12)}\,. \tag{C.19}$$

For $gg \to q\bar{q}$ we have

$$\mathcal{C}^{gg\to q\bar{q}} = \begin{pmatrix} C_F\Gamma^{(12)} + C_A\Gamma^{(ab)} & 0 & \frac{1}{2}(\beta+\gamma) \\ 0 & \chi'' & \frac{N_c}{4}(\beta+\gamma) \\ (\beta+\gamma) & \frac{N_c^2-4}{4N_c}(\beta+\gamma) & \chi'' \end{pmatrix}. \tag{C.20}$$

The signs are

$$\mathcal{S}_\alpha = +1\,, \tag{C.21}$$
$$\mathcal{S}_\beta = +1\,, \tag{C.22}$$
$$\mathcal{S}_\gamma = -1\,, \tag{C.23}$$

and we define

$$\chi'' = \frac{N_c}{4}(\beta-\gamma) - \frac{1}{2N_c}\Gamma^{(12)} + \frac{N_c}{2}\Gamma^{(ab)}\,. \tag{C.24}$$

The process $gg \to gg$.

$$\mathcal{C}^{gg\to gg} = \begin{pmatrix} \mathcal{M}_{3\times3} & 0_{3\times5} \\ 0_{5\times3} & \mathcal{M}_{5\times5} \end{pmatrix}, \tag{C.25}$$

where the matrix $\mathcal{M}_{3\times3}$ is

$$\mathcal{M}_{3\times3} = \begin{pmatrix} \frac{N_c}{2}(\alpha+\beta) & 0 & 0 \\ 0 & \frac{N_c}{2}(\alpha-\gamma) & 0 \\ 0 & 0 & \frac{N_c}{2}(\beta-\gamma) \end{pmatrix}, \tag{C.26}$$

and the matrix $\mathcal{M}_{5\times5}$ is

$$\mathcal{M}_{5\times5} = \begin{pmatrix} 3\beta & 0 & 3(\alpha+\gamma) & 0 & 0 \\ 0 & \frac{3}{4}(\alpha+2\beta-\gamma) & \frac{3}{4}(\alpha+\gamma) & \frac{3}{2}(\alpha+\gamma) & 0 \\ \frac{3}{8}(\alpha+\gamma) & \frac{3}{4}(\alpha+\gamma) & \frac{3}{4}(\alpha+2\beta-\gamma) & 0 & \frac{9}{8}(\alpha+\gamma) \\ 0 & \frac{3}{5}(\alpha+\gamma) & 0 & \frac{3}{2}(\alpha-\gamma) & \frac{9}{10}(\alpha+\gamma) \\ 0 & 0 & \frac{1}{3}(\alpha+\gamma) & \frac{2}{3}(\alpha+\gamma) & 2\alpha-\beta-2\gamma \end{pmatrix}, \tag{C.27}$$

for $N_c = 3$. The signs are

$$\mathcal{S}_\alpha = +1\,, \tag{C.28}$$
$$\mathcal{S}_\beta = +1\,, \tag{C.29}$$
$$\mathcal{S}_\gamma = -1\,. \tag{C.30}$$

JHEP09(2003)056

The direct processes. This processes has no matrix structure.

$$\begin{aligned}
\mathcal{C}^{\gamma g\to q\bar{q}} &= -\frac{1}{2N_c}\Gamma^{(12)} + \frac{N_c}{2}\left(\Gamma^{(b1)} + \Gamma^{(b2)}\right), \\
\mathcal{C}^{\gamma q\to gq} &= -\frac{1}{2N_c}\Gamma^{(b2)} + \frac{N_c}{2}\left(\Gamma^{(b2)} + \Gamma^{(12)}\right). \qquad \text{(C.31)}
\end{aligned}$$

D. The $\Gamma^{(ij)}$ series expansions

We have not found a closed form for these integrals, but they are straightforward to express as power series in R and $e^{-\Delta\eta}$ (by Lorentz invariance, only the contributions from dipoles containing jet 2 are $\Delta\eta$-dependent),

$$\Omega_1^{(ab)} = \frac{\alpha_s}{\pi}\left(\frac{1}{4}R^2\right), \qquad \text{(D.1)}$$

$$\begin{aligned}
\Omega_1^{(12)} = \frac{\alpha_s}{\pi}\Bigg(&\frac{1}{2}\log R + \frac{1}{2}\log\frac{1}{\Delta\eta - \Delta y} + \\
&+ (+0.31831\,R + 0.06250\,R^2 + 0.00884\,R^3 + 0.00087\,R^4 + 0.00003\,R^5) + \\
&+ (-0.08616\,R - 0.03383\,R^2 - 0.01197\,R^3 - 0.00282\,R^4 - \\
&\quad - 0.00039\,R^5 + 0.00001\,R^7)e^{-(\Delta\eta-2)} + \\
&+ (+0.01166\,R + 0.00916\,R^2 + 0.00551\,R^3 + 0.00305\,R^4 + \\
&\quad + 0.00122\,R^5 + 0.00038\,R^6 + 0.00011\,R^7 + 0.00003\,R^8)e^{-2(\Delta\eta-2)} + \\
&+ (-0.00158\,R - 0.00186\,R^2 - 0.00162\,R^3 - 0.00139\,R^4 - 0.00088\,R^5 - \\
&\quad - 0.00041\,R^6 - 0.00017\,R^7 - 0.00007\,R^8 - 0.00002\,R^9)e^{-3(\Delta\eta-2)} + \\
&+ (+0.00021\,R + 0.00034\,R^2 + 0.00039\,R^3 + 0.00045\,R^4 + \\
&\quad + 0.00039\,R^5 + 0.00024\,R^6 + 0.00013\,R^7 + 0.00007\,R^8 + \\
&\quad + 0.00003\,R^9 + 0.00001\,R^{10})e^{-4(\Delta\eta-2)} + \\
&+ (-0.00003\,R - 0.00006\,R^2 - 0.00008\,R^3 - 0.00012\,R^4 - \\
&\quad - 0.00013\,R^5 - 0.00010\,R^6 - 0.00007\,R^7 - 0.00004\,R^8 - \\
&\quad - 0.00003\,R^9 - 0.00001\,R^{10})e^{-5(\Delta\eta-2)} + \\
&+ (+0.00001\,R^2 + 0.00002\,R^3 + 0.00003\,R^4 + 0.00004\,R^5 + \\
&\quad + 0.00003\,R^6 + 0.00003\,R^7 + 0.00002\,R^8 + 0.00001\,R^9)e^{-6(\Delta\eta-2)}\Bigg), \qquad \text{(D.2)}
\end{aligned}$$

$$\begin{aligned}
\Omega_1^{(a1)} = \frac{\alpha_s}{\pi}\Bigg(&\frac{1}{2}\log R + \frac{1}{2}\log\frac{1}{\Delta\eta - \Delta y} - \\
&- 0.31831\,R + 0.06250\,R^2 - 0.00884\,R^3 + 0.00087\,R^4 - 0.00003\,R^5\Bigg), \qquad \text{(D.3)}
\end{aligned}$$

$$\begin{aligned}
\Omega_1^{(b2)} = \frac{\alpha_s}{\pi}\Bigg(&(+0.00458\,R^2 + 0.00389\,R^3 + 0.00229\,R^4 + 0.00104\,R^5 + \\
&\quad + 0.00038\,R^6 + 0.00012\,R^7 + 0.00003\,R^8)e^{-2(\Delta\eta-2)} + \\
&+ (-0.00124\,R^2 - 0.00158\,R^3 - 0.00124\,R^4 - 0.00079\,R^5 \\
&\quad - 0.00041\,R^6 - 0.00018\,R^7 - 0.00007\,R^8 - 0.00002\,R^9)e^{-3(\Delta\eta-2)} +
\end{aligned}$$

$$
\begin{aligned}
&+ (+0.00025\,R^2 + 0.00043\,R^3 + 0.00042\,R^4 + 0.00034\,R^5 + 0.00024\,R^6 + \\
&\quad + 0.00014\,R^7 + 0.00007\,R^8 + 0.00003\,R^9 + 0.00001\,R^{10})e^{-4(\Delta\eta-2)} + \\
&+ (-0.00005\,R^2 - 0.00010\,R^3 - 0.00011\,R^4 - 0.00011\,R^5 - 0.00010\,R^6 - \\
&\quad - 0.00007\,R^7 - 0.00004\,R^8 - 0.00002\,R^9 - 0.00001\,R^{10})e^{-5(\Delta\eta-2)} + \\
&+ (+0.00002\,R^3 + 0.00003\,R^4 + 0.00003\,R^5 + \\
&\quad + 0.00003\,R^6 + 0.00003\,R^7 + 0.00002\,R^8 + 0.00001\,R^9)e^{-6(\Delta\eta-2)}\Big) , \qquad \text{(D.4)}
\end{aligned}
$$

$$
\begin{aligned}
\Omega_1^{(a2)} = \frac{\alpha_s}{\pi}\Big(&- \frac{1}{4}R^2 + (+0.06767\,R^2 + 0.02872\,R^3 - 0.00096\,R^5 + 0.00002\,R^7)e^{-(\Delta\eta-2)} + \\
&+ (-0.01374\,R^2 - 0.01166\,R^3 - 0.00229\,R^4 - 0.00038\,R^6 - \\
&\quad - 0.00021\,R^7 - 0.00003\,R^8)e^{-2(\Delta\eta-2)} + \\
&+ (+0.00248\,R^2 + 0.00316\,R^3 + 0.00124\,R^4 + 0.00032\,R^5 + \\
&\quad + 0.00041\,R^6 + 0.00027\,R^7 + 0.00007\,R^8 + 0.00001\,R^9)e^{-3(\Delta\eta-2)} + \\
&+ (-0.00042\,R^2 - 0.00071\,R^3 - 0.00042\,R^4 - 0.00019\,R^5 - 0.00024\,R^6 - \\
&\quad - 0.00019\,R^7 - 0.00007\,R^8 - 0.00002\,R^9 - 0.00001\,R^{10})e^{-4(\Delta\eta-2)} + \\
&+ (+0.00007\,R^2 + 0.00014\,R^3 + 0.00011\,R^4 + 0.00007\,R^5 + 0.00010\,R^6 + \\
&\quad + 0.00009\,R^7 + 0.00004\,R^8 + 0.00002\,R^9 + 0.00001\,R^{10})e^{-5(\Delta\eta-2)} + \\
&+ (-0.00001\,R^2 - 0.00003\,R^3 - 0.00003\,R^4 - 0.00002\,R^5 - \\
&\quad - 0.00003\,R^6 - 0.00004\,R^7 - 0.00002\,R^8 - 0.00001\,R^9)e^{-6(\Delta\eta-2)}\Big) , \qquad \text{(D.5)}
\end{aligned}
$$

$$
\begin{aligned}
\Omega_1^{(b1)} = \frac{\alpha_s}{\pi}\Big(&-\frac{1}{2}\log R - \frac{1}{2}\log\frac{1}{\Delta\eta - \Delta y} - \\
&- 0.31831\,R - 0.06250\,R^2 - 0.00884\,R^3 - 0.00087\,R^4 - 0.00003\,R^5\Big) , \qquad \text{(D.6)}
\end{aligned}
$$

where all coefficients larger than 10^{-5} are shown (recall that we are mainly interested in the case $R = 1$, $\Delta\eta > 2$). By symmetry, we have $\Omega_2^{(ij)} = \Omega_1^{(\bar{\imath}\bar{\jmath})}$, where the mapping $i \to \bar{\imath}$ is given by $\{a, b, 1, 2\} \to \{b, a, 2, 1\}$.

E. The $\Omega_f^{(ij)}$ angular integrals for a cone geometry

We present these results as they have not appeared previously in this form. They have the expression,

$$
\Omega_f^{(ij)} = \int_{-\Delta y/2}^{+\Delta y/2} d\eta \int_0^{2\pi} \frac{d\phi}{2\pi} \frac{\beta_i \cdot \beta_j}{(\beta_i \cdot \bar{k})(\beta_j \cdot \bar{k})} , \qquad \text{(E.1)}
$$

where the integrand is found from the appropriate 4-momenta, and the phase space is taken to be of width Δy and azimuthally symmetric. Note that these expressions do not include the sign factors. We obtain

$$
\begin{aligned}
\Omega_f^{(ab)} &= 2\Delta y , \\
\Omega_f^{(12)} &= 2\log\left(\frac{\sinh(\Delta\eta/2 + \Delta y/2)}{\sinh(\Delta\eta/2 - \Delta y/2)}\right) ,
\end{aligned}
$$

JHEP09(2003)056

$$
\begin{aligned}
\Omega_f^{(a1)} &= -\Delta y + \log\left(\frac{\sinh(\Delta\eta/2+\Delta y/2)}{\sinh(\Delta\eta/2-\Delta y/2)}\right), \\
\Omega_f^{(b2)} &= -\Delta y + \log\left(\frac{\sinh(\Delta\eta/2+\Delta y/2)}{\sinh(\Delta\eta/2-\Delta y/2)}\right), \\
\Omega_f^{(a2)} &= \Delta y + \log\left(\frac{\sinh(\Delta\eta/2+\Delta y/2)}{\sinh(\Delta\eta/2-\Delta y/2)}\right), \\
\Omega_f^{(b1)} &= \Delta y + \log\left(\frac{\sinh(\Delta\eta/2+\Delta y/2)}{\sinh(\Delta\eta/2-\Delta y/2)}\right).
\end{aligned} \tag{E.2}
$$

References

[1] G. Marchesini and B.R. Webber, *Associated transverse energy in hadronic jet production*, *Phys. Rev.* **D 38** (1988) 3419.

[2] Yu.L. Dokshitzer, V. Khoze and S. Troyan, in *Physics in collision VI*, Proceedings of the International Conference, Chicago, Illinois, 1986, M. Derrick ed., World Scientific, Singapore 1987, p. 365.

[3] J.D. Bjorken, *Rapidity gaps and jets as a new physics signature in very high-energy hadron hadron collisions*, *Phys. Rev.* **D 47** (1993) 101.

[4] ZEUS collaboration, M. Derrick et al., *Rapidity gaps between jets in photoproduction at HERA*, *Phys. Lett.* **B 369** (1996) 55 [hep-ex/9510012].

[5] ZEUS collaboration, *Rapidity gaps between jets in photoproduction at HERA*, The XXXIth International Conference on High Energy Physics, Amsterdam, July 2002 Abstract number 852.

[6] H1 collaboration, C. Adloff et al., *Energy flow and rapidity gaps between jets in photoproduction at HERA*, *Eur. Phys. J.* **C 24** (2002) 517 [hep-ex/0203011].

[7] N. Kidonakis, G. Oderda and G. Sterman, *Threshold resummation for dijet cross sections*, *Nucl. Phys.* **B 525** (1998) 299 [hep-ph/9801268].

[8] N. Kidonakis, G. Oderda and G. Sterman, *Evolution of color exchange in QCD hard scattering*, *Nucl. Phys.* **B 531** (1998) 365 [hep-ph/9803241].

[9] G. Oderda and G. Sterman, *Energy and color flow in dijet rapidity gaps*, *Phys. Rev. Lett.* **81** (1998) 3591 [hep-ph/9806530].

[10] G. Oderda, *Dijet rapidity gaps in photoproduction from perturbative QCD*, *Phys. Rev.* **D 61** (2000) 014004 [hep-ph/9903240].

[11] C.F. Berger, T. Kúcs and G. Sterman, *Energy flow in interjet radiation*, *Phys. Rev.* **D 65** (2002) 094031 [hep-ph/0110004].

[12] M. Dasgupta and G.P. Salam, *Resummation of non-global QCD observables*, *Phys. Lett.* **B 512** (2001) 323 [hep-ph/0104277].

[13] M. Dasgupta and G.P. Salam, *Accounting for coherence in interjet E_T flow: a case study*, *J. High Energy Phys.* **03** (2002) 017 [hep-ph/0203009].

[14] R.B. Appleby and M.H. Seymour, *Non-global logarithms in inter-jet energy flow with kt clustering requirement*, *J. High Energy Phys.* **12** (2002) 063 [hep-ph/0211426].

[15] R.B. Appleby and G.P. Salam, *Theory and phenomenology of non-global logarithms*, presented at *38th Rencontres de Moriond on QCD and high-energy hadronic interactions*, Les Arcs, France, 22–29 March 2003 [hep-ph/0305232].

[16] J.C. Collins, D.E. Soper and G. Sterman, *Soft gluons and factorization*, *Nucl. Phys.* **B 308** (1988) 833.

[17] M.G. Sotiropoulos and G. Sterman, *Color exchange in near forward hard elastic scattering*, *Nucl. Phys.* **B 419** (1994) 59 [hep-ph/9310279].

[18] H. Contopanagos, E. Laenen and G. Sterman, *Sudakov factorization and resummation*, *Nucl. Phys.* **B 484** (1997) 303 [hep-ph/9604313].

[19] S. Catani, Y.L. Dokshitzer, M.H. Seymour and B.R. Webber, *Longitudinally invariant $k(t)$ clustering algorithms for hadron hadron collisions*, *Nucl. Phys.* **B 406** (1993) 187.

[20] S.D. Ellis and D.E. Soper, *Successive combination jet algorithm for hadron collisions*, *Phys. Rev.* **D 48** (1993) 3160 [hep-ph/9305266].

[21] J.M. Butterworth, J.P. Couchman, B.E. Cox and B.M. Waugh, *Ktjet: a C++ implementation of the $k(t)$ clustering algorithm*, *Comput. Phys. Commun.* **153** (2003) 85 [hep-ph/0210022].

[22] C.F. von Weizsäcker, *Radiation emitted in collisions of very fast electrons*, *Z. Phys.* **88** (1934) 612;
E.J. Williams, *Nature of the high-energy particles of penetrating radiation and status of ionization and radiation formulae*, *Phys. Rev.* **45** (1934) 729.

[23] N. Kidonakis and J.F. Owens, *Effects of higher-order threshold corrections in high-E_T jet production*, *Phys. Rev.* **D 63** (2001) 054019 [hep-ph/0007268].

[24] C.F. Berger, *Soft gluon exponentiation and resummation*, hep-ph/0305076.

[25] Y.L. Dokshitzer and G. Marchesini, *On large angle multiple gluon radiation*, *J. High Energy Phys.* **03** (2003) 040 [hep-ph/0303101].

[26] C.F. Berger, T. Kúcs and G. Sterman, *Event shape/energy flow correlations*, *Phys. Rev.* **D 68** (2003) 014012 [hep-ph/0303051].

[27] M. Gluck, E. Reya and A. Vogt, *Photonic parton distributions*, *Phys. Rev.* **D 46** (1992) 1973.

[28] A.D. Martin, R.G. Roberts, W.J. Stirling and R.S. Thorne, *Scheme dependence, leading order and higher twist studies of MRST partons*, *Phys. Lett.* **B 443** (1998) 301 [hep-ph/9808371].

[29] G. Corcella et al., *Herwig 6: an event generator for hadron emission reactions with interfering gluons (including supersymmetric processes)*, *J. High Energy Phys.* **01** (2001) 010 [hep-ph/0011363].

[30] G. Corcella et al., *Herwig 6.5 release note*, hep-ph/0210213.

[31] G.P. Korchemsky and G. Sterman, *Power corrections to event shapes and factorization*, *Nucl. Phys.* **B 555** (1999) 335 [hep-ph/9902341].

JHEP09(2003)056